Renewable Energy 211 (2023) 87–99

Contents lists available at ScienceDirect

Renewable Energy

journal homepage: www.elsevier.com/locate/renene

Thermal and fluid dynamic optimization of a CPV-T receiver for solar co-generation applications: Numerical modelling and experimental validation

Daniel Santos [a], Ahmet Azgın [b], Jesus Castro [a], Deniz Kizildag [a], Joaquim Rigola [a,*], Bilge Tunçel [e], Raşit Turan [d,f], Rupert Preßmair [c], Richard Felsberger [c], Armin Buchroithner [c]

[a] Centre Tecnològic de Transferència de Calor (CTTC), Universitat Politècnica de Catalunya (UPC), Terrassa, Barcelona, Spain
[b] İleri Arge Teknolojileri, Ankara, Turkey
[c] Institute of Electrical Measurement and Sensor Systems (EMS), Graz University of Technology (TUG), Graz, Austria
[d] Middle East Technical University-Centre for Solar Energy Research and Applications (ODTU-GÜNAM), Ankara, Turkey
[e] Energy Engineering, Ankara University, Ankara, Turkey
[f] Department of Physics, Middle East Technical University (METU), Ankara, Turkey

ARTICLE INFO

Keywords:
Concentrated photoVoltaic thermal system
Computational fluid dynamics
Solar energy
Solar cells
Receiver
Heat sink

ABSTRACT

Solar co-generation, i.e., the generation of electricity and heat in a single device by concentrating the sunbeams, has the potential to significantly increase the overall system performance. The main challenge is related to the cooling of solar cells. In order to do so, it is essential to reduce the thermal resistance between the cell and heat transfer fluid. This paper features the optimization procedure of a low-cost custom concentrated photovoltaic thermal (CPV-T) receiver for a parabolic trough collector using silicon solar cells. A finite volume model for the thermal process has been developed. Hence, a fluid dynamic thermal simulation of the receiver is presented. The optimized heat sink tube geometries have been manufactured and tested in a lab environment, allowing for a comparison between modelling and experimental test results. Three possible heat sink geometries have been designed and compared regarding their overall heat transfer coefficient with respect to the non-dimensional pumping power, i.e. the ratio between the overall transferred heat and the energy required for pumping. The overall heat transfer coefficient for a finned heat sink has been increased up to 60% with respect to a baseline case without fins under similar conditions.

1. Introduction

Solar energy is one of the cheapest, cleanest, and most abundant renewable energy sources and the only one capable of being used for heating or cooling and electrical power generation at the same time [1]. Concentrated photovoltaic thermal (CPV-T) systems reduce the cell area and due cost, focusing the beam solar energy to produce electrical power. Therefore, the thermal receiver can extract the waste heat reducing the cell temperature and increasing the electricity generated. The system variations and technological advances in CPV-T, together with thermal and electrical efficiencies of various CPV-T applications, were described by Sharaf et al. [2,3]. Ju et al. [4,5] presented a systematic review on CPV-T of different concentration levels (low, medium, and high), highlighting the CPV-T systems for building integration, poly-generation, cooling, and desalination applications. Daneshazarian et al. [6] summarized the experimental and theoretical investigations on CPV-T found in the literature. This reference reported the maximum efficiencies achieved in this technology, i.e. 70% of total efficiency and 25% of electrical efficiency, using parabolic through collectors. Moreover, a value of electricity cost of 2.37 $/W and 8.7 $/W for the total electrical and thermal costs were also reported.

Moreover, Kasaeian et al. [7] reviewed CPV-T with trough/Fresnel concentrators, identifying research gaps, as they are less developed than parabolic CPVT. Besides, a recent publication presents CPV-T applications of parabolic trough using simple modelling and experimental validation in [8] and experimental flow regimes and concentration ratios analysis in [1]. These two last articles identified research needs, mainly focused on price reduction, such as integration of components (e.g., storage, thermal cycles -Kalina-, etc.), and also reduction of the price through Heat transfer enhancement in the heat sink.

Concerning the heat sink design, there are many works in the literature. Papis-Fraçzeka and Sornek [9] reviewed the heat sink de-

* Corresponding author.
E-mail address: joaquim.rigola@upc.edu (J. Rigola).

https://doi.org/10.1016/j.renene.2023.04.064
Received 2 December 2022; Received in revised form 1 April 2023; Accepted 14 April 2023
Available online 20 April 2023

Nomenclature

A	Heat transfer area [m^2]
CAM	Cogeneration Absorber Module or receiver
CFD	Computational Fluid Dynamics
c_p	Heat capacity at constant pressure [J/kg K]
CPV-T	Concentrated photovoltaic thermal system
CT	Cell Tray or CPV Mounting Plate
g	Gravity acceleration vector [m/s^2]
HS	Heat sink
HTF	Heat Transfer Fluid
$\dot{m}$	Mass flow rate [kg/s]
N	Number of control volumes
OTS	Off-the-shelf
p	Pressure [Pa]
PR	Plate Resistance
$\dot{Q}$	Total heat entering the system [W]
QC	Quarter Cut
$\dot{Q}_f$	Heat absorbed by the fluid [W]
R	Rectangular Pipe without fins
RO	Rectangular Pipe with off-the-shelf heat sink
$\mathbf{S}_t$	Source term
T	Temperature [°C]
T_0	Reference temperature [°C]
T_{CT}	Average temperature of the CT [°C]
T_{CT-PR}	Average temperature of the CT-PR boundary [°C]
T_{CT-HS}	Average temperature of the CT-HS boundary [°C]
T_{HTF}	Average temperature of the HTF [°C]
T_{in}	Inlet fluid temperature [°C]
T_{out}	Outlet fluid temperature [°C]
T_{PR}	Average temperature of the PR [°C]
u	Velocity vector [m/s]
U	Global heat transfer coefficient [W/m^2 K]
x, y, z	Cartesian coordinates

Greek symbols

β	Thermal expansion coefficient [K^{-1}]
Δp	Pressure drop [Pa]
ΔT	Inlet and outlet fluid temperatures difference [K]
κ	Thermal conductivity [W/m^2 K]
ρ	Density [kg/m^3]
ν	Kinematic viscosity [m^2/s]

velopments for CPV-T applications. They classify the heat sinks into (i) macro-Scale based channels/ducts, including rectangular, circular, and triangular ducts, metal blocks with inner channels, serpentine ducts, and other designs, including cut circular or finned tubes; and (ii) micro-scale-based channels of different arrangements and geometries.

Concerning Heat Extraction Devices with Macro-Scale Channels/Ducts, there is much-published research. Rectangular tubes were used at Refs. [10–17], circular tubes in [18–25] and triangular tubes in [26–31]. However, in all these works, only values of the overall thermal and electrical performances of the CPVT are provided. Therefore, there has been detected a lack of optimization studies for this type of heat sink, as no special heat transfer enhancements were used, except in the Refs. [32–34], in which grooved tubes were employed.

On the other hand, the optimization studies for heat sinks have been focused on geometries based on rectangular microchannels. [35] perform research for a heat sink for electronics heat dissipation. They reported an overall heat transfer coefficient of about 1600 W/K and ratios between heat dissipated/pumping power of about 400–5000. Moreover, the research performed by [36] reported an overall heat transfer coefficient of about 50 W/K and heat dissipated/pumping power ratios of about 60 000. In the particular case of [37], a channel with variable fins in the fluid direction is designed and then experimentally assessed in [38,39]. They achieve an overall transfer coefficient in the heat sink of 70–121 W/K, with values of heat dissipated divided by pumping power of about 20 000. Their prototype system achieved thermal and electrical efficiency in the order of 44% and 6%, respectively (with monocrystalline silicon PV cells). In the case of [40], a trapezoidal section of the heat sink channels is also considered, achieving a heat transfer coefficient for the heat sink in the range of 70–125 W/K, with a pumping power of about 0.4 W (in this work, the heat rejected by the heat sink was not provided). A different approach was performed by Rahmanian et al. research [41]. Their work was focused on enhancing heat transfer by modifying the heat transfer fluid (HTF) using PCM with nanoparticles, achieving a thermal efficiency of 45%, an electrical efficiency near 14% (using a silicon PV cell), at a temperature of 30 °C of nanofluid, and 45 °C for the PV cell. In summary, most studies based on microchannel heat sinks are focused on performance enhancement/optimization to achieve high-performance results but are based on ad-hoc constructive solutions independently of the final price.

The development of hybrid absorbers usually involves expensive high-performance multi-junction solar cells. For this reason, this paper is involved in the research of cost reduction of generating electricity by heat co-generation via CPV-T system (see Fig. 1). Although the quantification of the final price is out of the scope of this work, at the end of this research, a competitive price of the technology is expected due to the use of silicon-based cells and simplified construction techniques for the reflectors, structure, and heat sink. As the temperature coefficients of the silicon-based cells are inferior, the performance of the heat sink, i.e., its capability of keeping the temperature difference between the cell surface and HTF as small as possible, which means maximizing the global heat transfer coefficient, is of particular importance. Therefore, this work is focused on increasing the performance of a heat sink based on finned macro-scale rectangular/circular tubes using finned surfaces to obtain a higher amount of generated electricity while using thermal energy with the maximum possible temperature of the HTF.

The overall low-cost CPV-T system with an integrated hybrid absorber is shown in Fig. 2, taking advantage that the absorber tubes of thermal receivers being industrially standardized. Solar radiation is captured in a parabolic trough concentrator based on a novel injection moulding structure and focused on a Co-Generation Absorber Module (CAM), where special c-Si photovoltaic (PV) cells are operated under concentration. The heat dissipated through the cells is transferred into a heat transfer fluid (HTF). Therefore, in combination with electricity production, the CPV-T device can be used for various applications, such as solar cooling or heating [42]. The electrical and thermal optimal performances have a relevant double function: absorbing the maximum quantity of waste heat at the highest possible temperature for the thermal applications and minimizing the PV cell temperature, allowing it to give the maximum electrical efficiency. In order to achieve an optimum design of the low-cost CVP-T receiver, a CFD numerical model is used. The numerical model is validated using experimental results of laboratory tests of the receivers. Finally, a simple comparison is performed between the most promising designs using the CFD numerical simulation model, based on the ratio between heat transfer and pumping power needed, as many mass flow rates are evaluated, allowing easy comparison between different designs. The resulting simulations' results show that highly significant increase in the overall heat transfer coefficient for the finned heat sinks, from 30 to 60%, with respect to a reference case of a heat sink tube without fins.

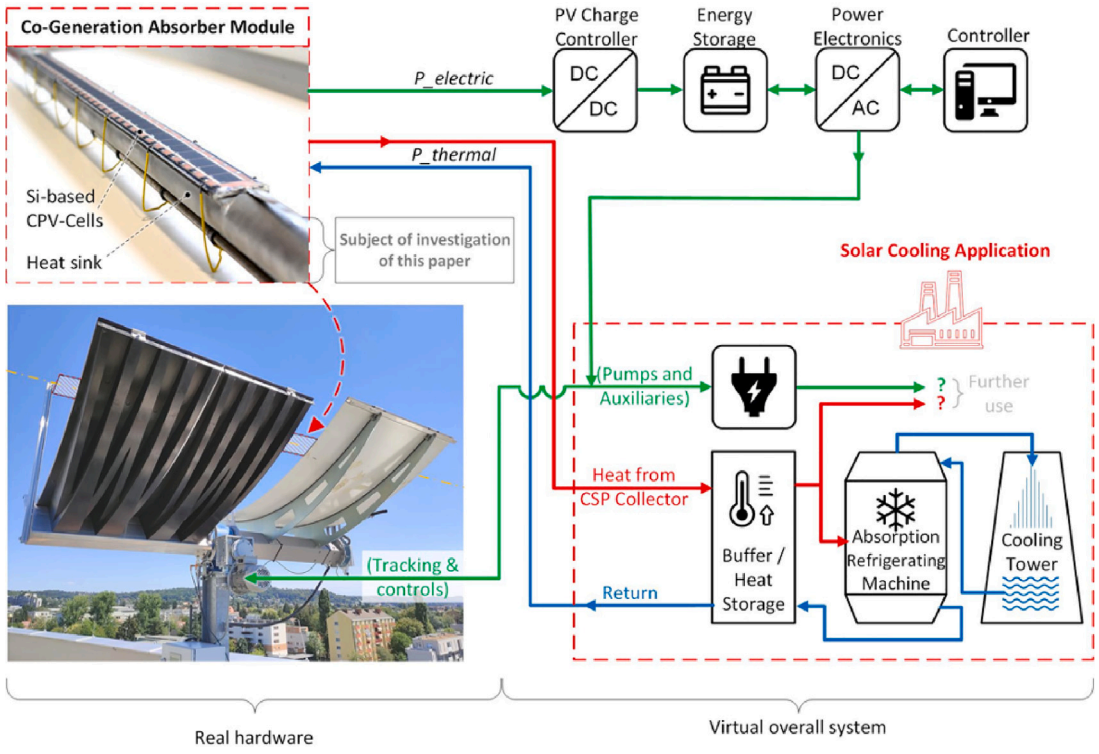

Fig. 1. Co-generation CPV-T system overview.

2. Numerical model and verification

Navier–Stokes and energy conservation equations are the governing physics of the CPV-T systems modelling. The main problem with these equations is that an analytical solution is not known for general cases. One powerful resource to obtain numerical solutions to the equations is Computational Fluid Dynamics (CFD) [43]. A model was structured to simulate the system and produce the numerical solutions using this procedure, which are approximate solutions of the equations, whose accuracy will depend on the methodology applied. Experimental data was used to assess the accuracy of the model. The validated model can, in turn, replace excessive experiments with varying conditions, like changing inlet conditions or geometry, which can be very expensive and laborious. The 3D model used in this work to simulate the experiments was previously validated using data published in [44,45], and [46].

This conjugate heat transfer model consists of solving (incompressible) Navier–Stokes equations with the Boussinesq approximation for fluid parts of the system, along with the energy conservation equation:

$$\nabla \cdot \mathbf{u} = 0 \tag{1}$$

$$\frac{\partial \mathbf{u}}{\partial t} + (\mathbf{u} \cdot \nabla)\mathbf{u} = \frac{1}{\rho}\nabla(p - \rho \mathbf{g}\mathbf{z}) + \nu\nabla^2\mathbf{u} - \mathbf{g}\beta(T - T_0) \tag{2}$$

$$\frac{\partial T}{\partial t} + \mathbf{u} \cdot \nabla T = \frac{\kappa}{\rho c_p}\nabla^2 T + \mathbf{S}_t \tag{3}$$

and conduction equation for solids:

$$\frac{\partial T}{\partial t} = \frac{\kappa}{\rho c_p}\nabla^2 T + \mathbf{S}_t \tag{4}$$

These equations are coupled at the solid–fluid interfaces, assuming that the heat flux exiting one domain enters the adjacent one and the temperature at the interface is the same for adjacent domains. Fig. 3 shows the flow chart of the numerical algorithm.

2.1. Independence of the solution regarding mesh size

OpenFOAM [47] is the code used to perform the simulations, specifically the "chtMultiRegionFoam" conjugate heat transfer solver, based on a collocated finite-volume discretization of the equations. The model is adopted to three different designs of the heat sinks, thoroughly explained and tested. Fig. 4 is the test configuration used to test the independence of the solution with regard to the mesh size.

In order to test the independency of the solution regarding the mesh size, specific simulations were carried out, progressively increasing the number of control volumes in x, y, and z directions until obtaining an asymptotic solution. The mesh is non-regular, i.e., the size of the control volumes is not constant. Fig. 5 shows Mesh A at the entrance of the rectangular pipe, and Table 1 shows the finer meshes tested for the rectangular pipe without fins case, with a mass flow rate of 6 L/min.

As can be observed in Table 1, results for the different selected temperatures show differences up to 6% between meshes A and B, and only differences of about 1% between meshes B and C are observed. Therefore, mesh B has been considered optimal for the following numerical cases due to computational power requirements.

Table 1
Different numerical temperature values depending on the number of control volumes for each tested meshes.

	NCV	T_{PR}	T_{CT}	T_{CT-PR}	T_{CT-HS}	T_{HTF}
Mesh A	576 000	43.072	46.343	45.197	41.747	16.934
Mesh B	1 452 000	41.882	45.783	44.308	39.370	16.785
Mesh C	2 366 000	41.622	46.173	44.668	38.950	16.705

3. Experimental test setup

The experimental setup for thermal performance testing of the designed CPV-T solar collector receiver is given in Fig. 6. Fig. 7 shows a schematic representation of the system.

The CPV Mounting Plate and heater are connected to the heat sink with clamps. To reduce the contact resistance between components, a standard thermal paste of a thermal conductivity $\kappa = 2.9$ W/m^2 K is applied to the surfaces see Fig. 8. The temperature sensors employed below the pipe were placed into half-way drilled thin channels on

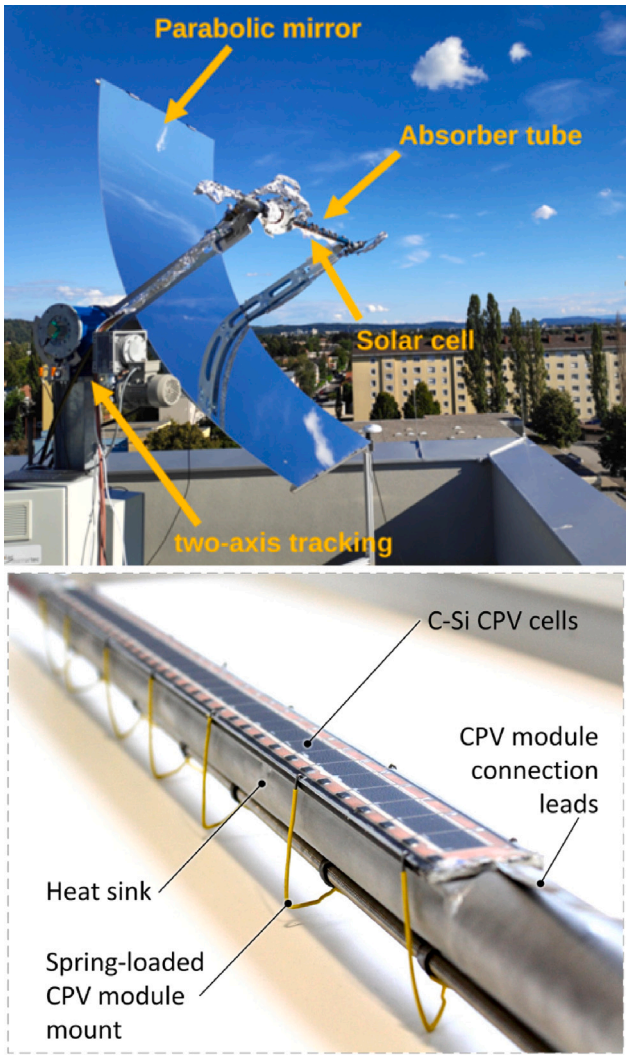

Fig. 2. (Top) Overview of the CPV-T system. (Bottom) Overview of the co-generation absorber module.

the CPV Mounting Plate with metal epoxy glue, Fig. 8b. The CPV-T pipe was enclosed by a regular Polypropylene Random Copolymer (PPRC) water pipe to insulate it. Inlet water comes from the building's plumbing system. Supply pressure was enough to drive the water through the setup, so there was no need for extra pumping. Outlet water drained down to the building drainage system. The flow rate of the inlet water is adjusted by a manual valve at the end and measured by a flowmeter.

A total of 11 thermocouples AWG20 and AWG30 T-type with an accuracy of ±1 °C were used in the system: two for the inlet and outlet temperatures of the fluid, three to capture the temperature gradient of the insulation layer and two for each following location at the beginning, the middle and the end of the heat sink. The thermocouples within the CPV-T pipe are placed between the heat sink and CPV Mounting Plate and between CPV Mounting Plate and heater. The positions of the thermocouples are shown in detail in Fig. 9.

An adjustable DC power source KEYSIGHT N8761A 300 V/17 A 5100 W provides the power for the heater. The heater is used as a heat source entering the system by transferring heat through plate thermal resistance instead of solar radiation. The temperature measurements by the thermocouples are captured by a data acquisition device Agilent 34972A LXI with a measurement frequency of every 10 s.

The experiment took place in a large closed indoor environment, with the ambient conditions stable. The water flow, measured by KROHNE H250 M9, with an accuracy of ±2% under stabilized conditions, follows a one-meter-long path before the inlet water temperature measurements are carried out. Upon passing through the CPV-T receiver, the follow-up pipe is elevated about 150 mm to ensure no air presence in the receiver. The outlet temperature measurement is placed about one meter away from the receiver's end to ensure that the flow is conveniently mixed. The municipal water comes from underground pipes with a steady temperature value, and the desired water flow rate is achieved by manually adjusting the valve. The connected DC power source was preset at 214.0 V and 5.15 A to the plate resistance heater, which was then switched on, generating 1100 W. The plate resistance provides a constant rate of heat to the system.

The water flow and heating power were maintained until the system reached a steady-state condition, which was achieved within 40 min. The experiment was repeated for the three designs at the three different flow rates of 6 L/min, 8 L/min, and 10 L/min. A preliminary test was carried out with 6 L/min, suggesting a turbulent flow regime start (depending on the cross-section of the receiver structure), which in turn ensured an optimal heat rejection.

4. Results

Different heat sink geometries have been designed and produced to reach optimal heat transfer areas by adding fins along the tube. The additional fins not only increase the heat transfer but also increase the pressure drop. Thus, it is necessary to find an optimum distribution by looking for the maximum global heat transfer coefficient considering this pressure drop. Unlike the retrofit version of a conventional absorber tube mentioned in [45], the heat sinks discussed in this section are designed as an integral hybrid absorber. Three designs have been tested: (i) Rectangular pipe without fins; (ii) Rectangular pipe with fins, off-the-shelf heat sink; and (iii) Quarter cut with an optimized heat sink. They are 1160 mm in length, consisting of 200 mm circular pipe on each end, and have a solar cell area underneath, which is 760 mm long at its central region. Fig. 10 gives the details of the manufactured heat sinks. The rectangular case without fins has an aluminium material Al-6063 with thermal conductivity of about 200 W/m K; the rectangular case with fins has the same aluminium Al-6063 for the heat sink but aluminium Al-1050 with thermal conductivity of about 222 W/m K for the pipe, while the quarter cat with an optimized heat sink has a unique aluminium material Al-6061 with thermal conductivity of about 167 W/m K. A value of around 0.1 mm was selected for the thermal paste thickness [48]. Numerical results obtained for the experimental configurations are shown in Sections 4.1, 4.2 and 4.3, while a comparative discussion is presented in Section 4.4. Finally, a simulation of the quarter cut with an optimized heat sink considering the same aluminium thermal conductivity as the other cases are numerically presented in Section 4.5 for comparison purposes.

In order to test the robustness of the numerical method, the three flow rates used in the experiments were also simulated with the developed numerical model for each design.

4.1. Rectangular pipe without fins

Fig. 11 shows the temperature distribution at the steady state condition along the central axis line of the CPV Mounting Plate/plate resistance boundary and the CPV Mounting Plate/rectangular pipe without fin heat sink boundary. Each graph corresponds to flow rates of 6 L/min, 8 L/min, and 10 L/min, with an HTF inlet temperature of 15.10 °C, 14.27 °C and 14.17 °C, respectively. They show the gradient temperature inside the CPV Mounting Plate due to the effect of the thermal paste. It also indicates where the maximum temperature is located. As can be seen, the gradients of temperature are smaller at the beginning and the end, but they become significant towards the centre.

The curves present a quick temperature grow until 0.1 m, then it continues growing slower up to 0.65 m, and finally we find a temperature drop up to the end. The maximum difference of temperature found

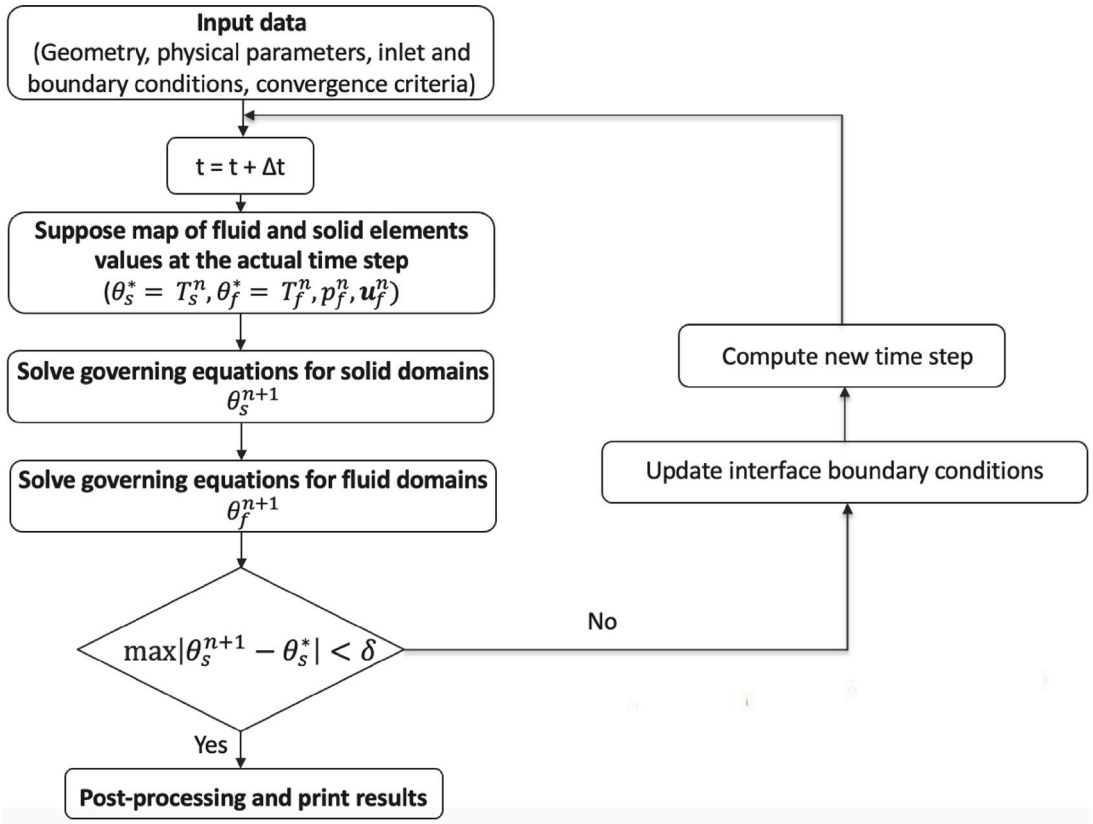

Fig. 3. Flow chart of the numerical algorithm.

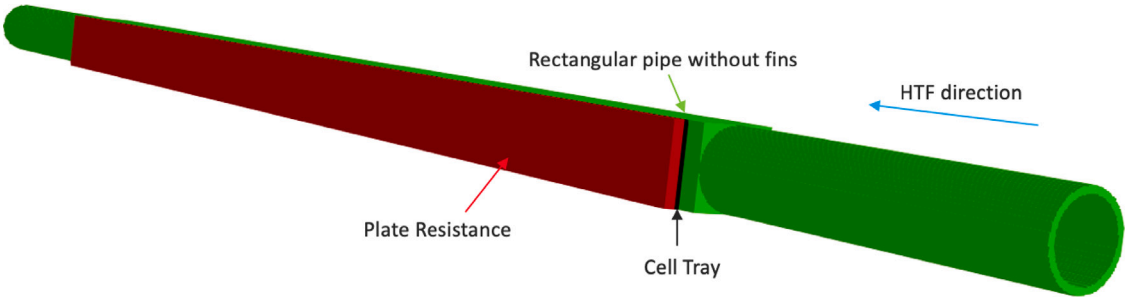

Fig. 4. Rectangular pipe configuration. Plate resistance and the Cell Tray position.

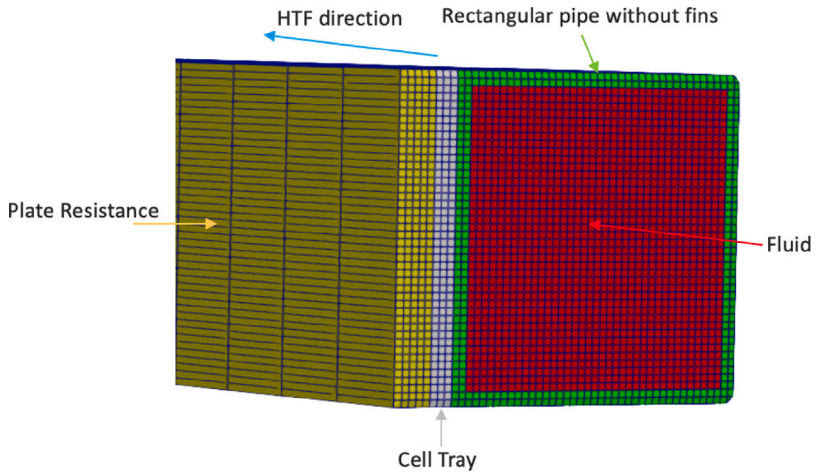

Fig. 5. Mesh A at the entrance of the rectangular pipe.

Fig. 6. The experimental set-up installed at the Mechanical Engineering Department of the Middle East Technical University, Turkey.

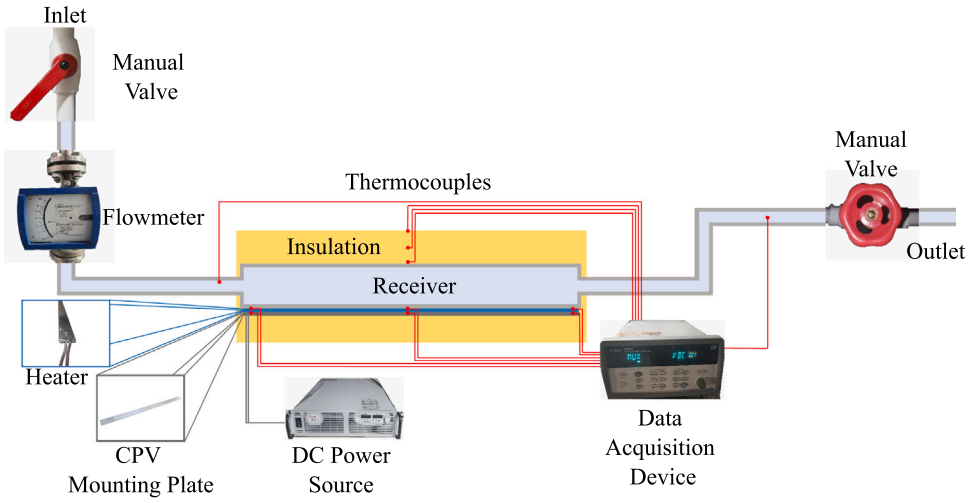

Fig. 7. General schematic representation of the experimental set-up.

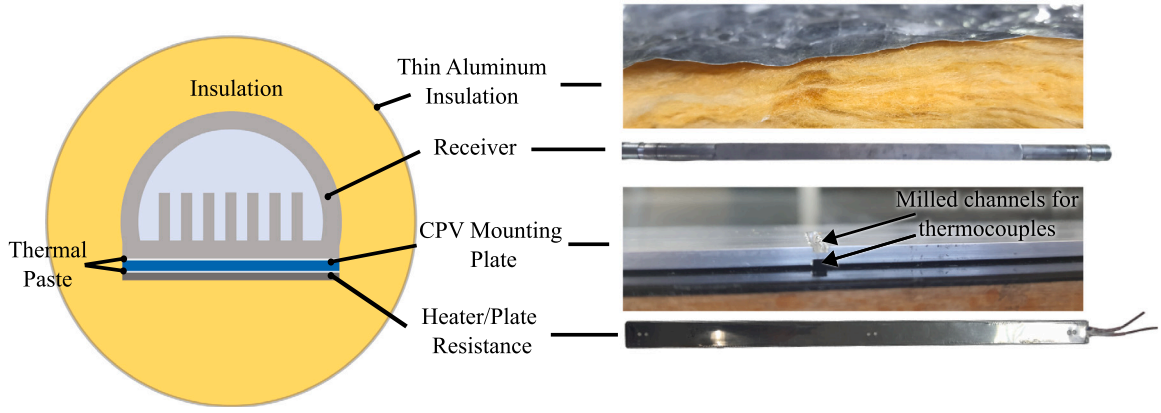

Fig. 8. Schematic representation of the cross-section of the set-up (left). The slots drilled on the CPV Mounting Plate for the thermocouple installation (right).

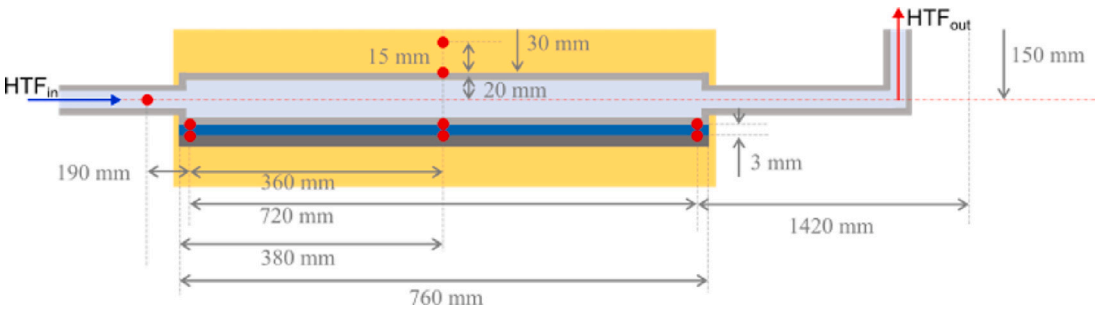

Fig. 9. The placement of the thermocouples on the experiment set-up. Red dots represent a thermocouple. Please note that the dimensions of the figure are not in scale.

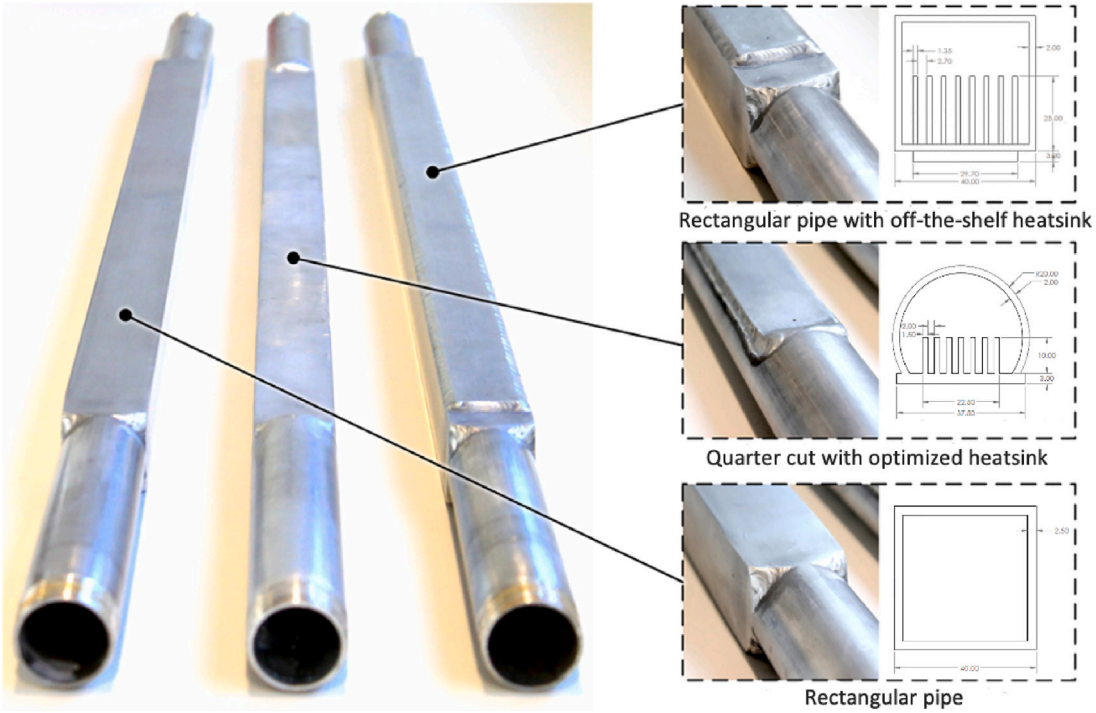

Fig. 10. Overview of the pipes tested in the simulations including the cross-section.

Table 2
Numerical comparison of the rectangular pipe for different mass flow rates.

Mass flow rate	T_{out} exp (°C)	T_{out} num (°C)	Δp (Pa)
6 L/min	17.70	17.66	8
8 L/min	16.13	16.25	13
10 L/min	15.64	15.81	20

Table 3
Numerical comparison of the rectangular pipe with fins for different mass flow rates.

Mass flow rate	T_{out} exp (°C)	T_{out} num (°C)	Δp (Pa)
6 L/min	17.85	17.78	19
8 L/min	16.80	16.93	31
10 L/min	15.85	16.02	44

inside the CPV for this range of mass flow rates is similar in the three cases, with a value of about 7 °C.

Table 2 shows the experimental and the numerical fluid temperature obtained at the outlet part of the pipe. Furthermore, the pressure drop is also included. The temperature discrepancies are between 0.04 °C and 0.17 °C. An increment of 25% of mass flow rate produces an increase of 40% on pressure drop.

4.2. Rectangular pipe with fins (off-the-shelf heat sink)

Fig. 12 shows the temperature distributions of the steady state along the central axis line of the CPV Mounting Plate, plate resistance boundary, CPV Mounting Plate, and heat sink boundary of the rectangular pipe with fins. Similarly, as above, each graph corresponds to different mass flow rates of 6 L/min, 8 L/min, and 10 L/min, with an HTF inlet temperature of 15.15 °C, 14.85 °C and 14.35 °C, respectively.

The curves present a quick temperature grow until 0.05 m, then it continues growing slower up to 0.4 m, showing a flat profile until 0.7 m and finally we find a temperature drop up to the end. This flat section was not found in the rectangular pipe without fins case. The maximum difference of temperature found inside the CPV for this range of mass flow rates is similar in the three cases, with a value of about 9 °C.

Table 3 shows the experimental and the numerical fluid temperature obtained at the outlet part of the pipe. Furthermore, the pressure drop is also included. The temperature discrepancies are around 0.07 °C to 0.17 °C. An increment of 25% of mass flow rate produces an increase of 40% on pressure drop.

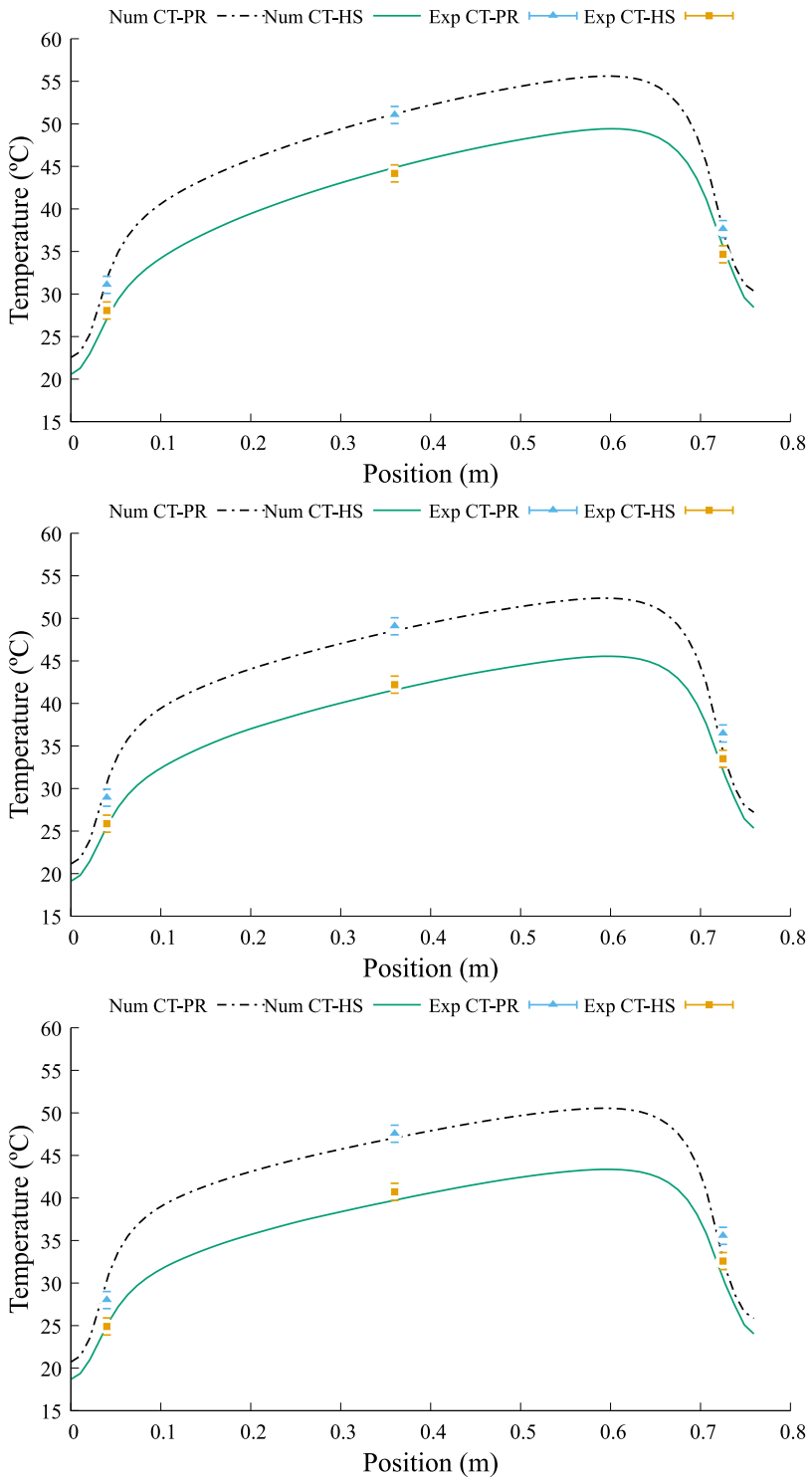

Fig. 11. PR-CT and CT-HS centre axis temperature of the rectangular pipe without fins with a mass flow rate of (top) 6 L/min, (middle) 8 L/min and (bottom) 10 L/min, respectively.

4.3. Quarter cut with optimized heat sink

Fig. 13 shows the temperature distributions of the steady state along the central axis line of the CPV Mounting Plate, plate resistance boundary, CPV Mounting Plate, and heat sink boundary of the quarter cut with fins. Similarly, as in the previous case, each graph corresponds to different mass flow rates of 6 L/min, 8 L/min, and 10 L/min, with an HTF inlet temperature of 15.4 °C, 16.41 °C and 16.41 °C, respectively.

The curves present a quick temperature grow until 0.05 m, then it continues growing slower up to 0.2 m, showing a flat profile until 0.7 m and finally we find a temperature drop up to the end. In contrast to the rectangular pipe with fins case, this flat profile appears before. The maximum difference of temperature found inside the CPV for this range of mass flow rates is similar in the three cases, with a value of about 8.3 °C, which is slightly lower than the value found for the rectangular pipe with fins case.

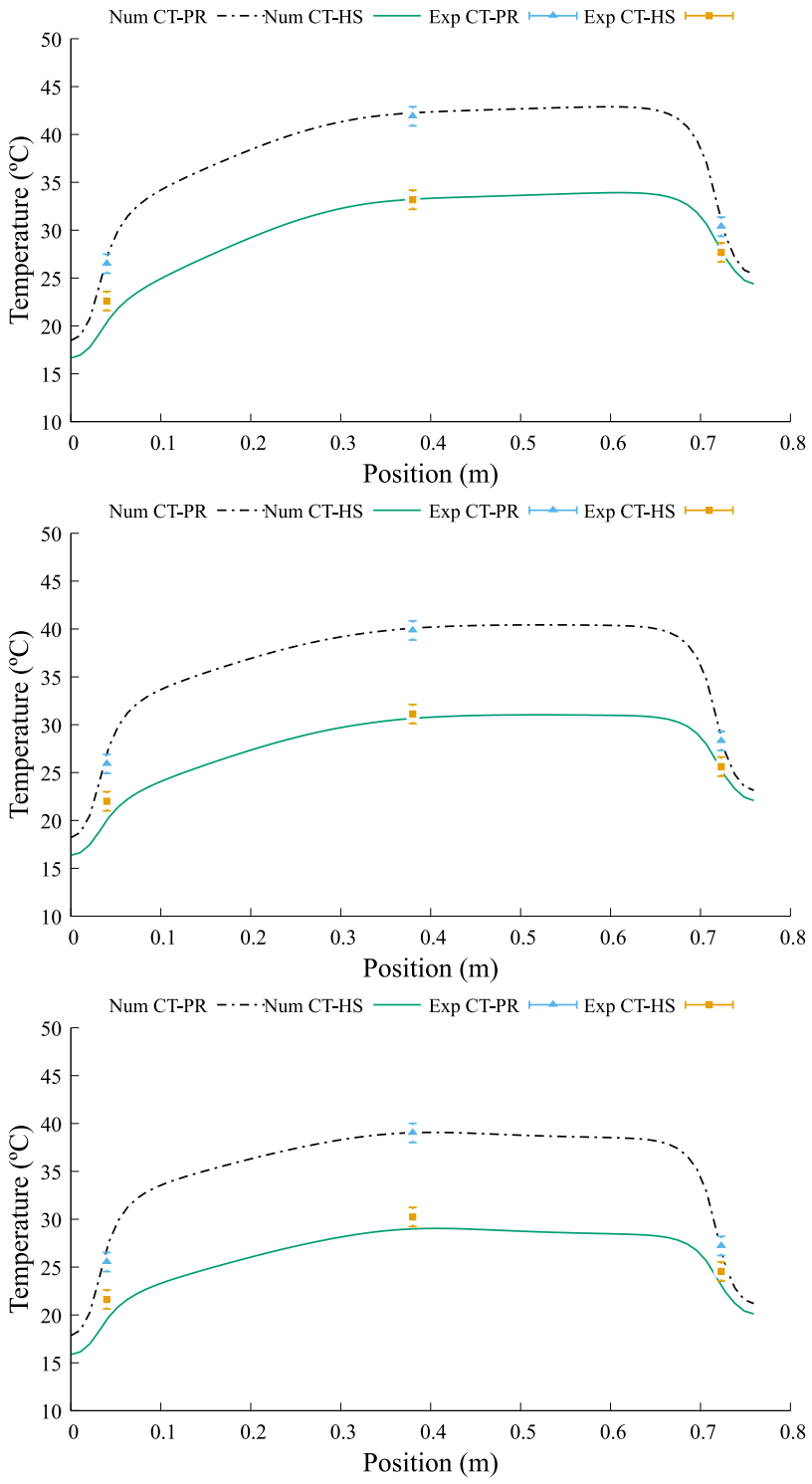

Fig. 12. PR-CT and CT-HS centre axis temperature of the rectangular pipe with fins with a mass flow rate of (top) 6 L/min, (middle) 8 L/min and (bottom) 10 L/min, respectively.

Table 4 shows the experimental and the numerical fluid temperature obtained at the outlet part of the pipe. Furthermore, the pressure drop is also included. The temperature discrepancies are around 0.10 °C to 0.15 °C. In this case, An increment of 25% of the mass flow rate produces an increase of 45% on pressure drop.

4.4. Conclusions of the numerical results

All numerical results shown have an acceptable agreement with the experimental ones, while discrepancies are always within the range of

Table 4
Numerical comparison of quarter cut with optimized heat sink for different mass flow rates.

Mass flow rate	T_{out} exp (°C)	T_{out} num (°C)	Δp (Pa)
6 L/min	19.05	19.15	31
8 L/min	17.90	18.05	48
10 L/min	17.55	17.70	64

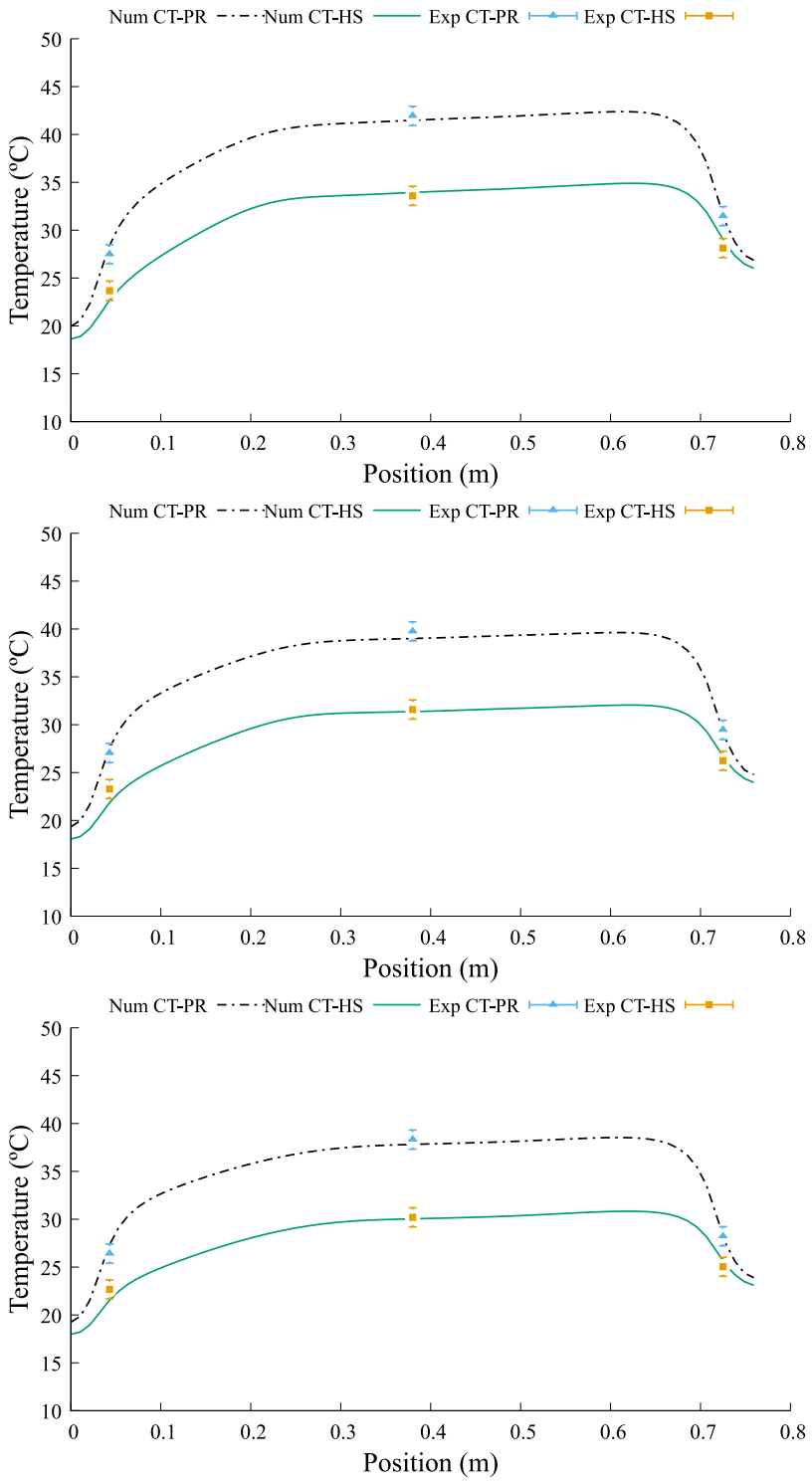

Fig. 13. PR-CT and CT-HS centre axis temperature of the quarter cut with fins with a mass flow rate of (top) 6 L/min, (middle) 8 L/min and (bottom) 10 L/min, respectively.

the experimental measurement's accuracy. Possible explanations for the differences observed can be related to experimental aspects such as: (i) There are some short design irregularities that the simulation is not able to capture, i.e., welding points and/or other thickness irregularities in the thermal paste layer; (ii) There is an imperfect homogeneous heat distribution due to the plate resistance; or (iii) There are slight inlet fluid temperature fluctuations not considered in the simulations. Additionally, from the numerical work: (i) Inherent errors due to the discretization and numerical schemes (particularly in zones with high-temperature gradients); (ii) Temperature comparisons have been done against mean steady-state values; or (iii) Thermal paste layer thickness inaccuracy.

The uncertainty of the thermal paste layer thickness has a relevant effect on the temperature and heat transfer distribution. In all cases, the CPV Mounting Plate has a 3 mm thickness, and the plate resistance has a 5 mm thickness. Therefore, a thermal paste layer of around 0.1 mm influences the results. The equivalent thermal conductivity essentially depends on the thermal paste layer thickness because its thermal conductivity is very low. A small error in measuring the thermal layer thickness, which is difficult to measure due to its size, may lead to a

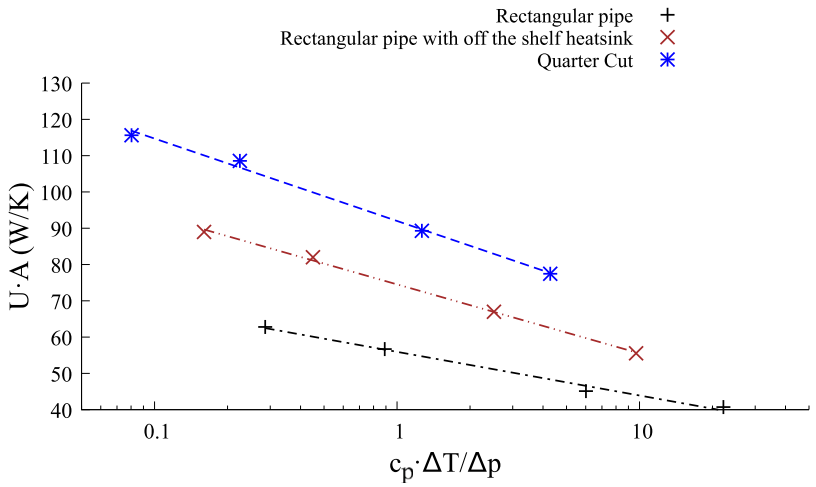

Fig. 14. Graph comparing the three different designs. Horizontal axis is in logarithmic. Logarithmic trend lines are included.

significant change in the thermal conductivity of the piece. In addition, this thermal paste layer is not flat in the actual experiment, which cannot be considered in the simulation.

4.5. Performance comparison

As it is difficult to analyse the best-performing design from the temperature graphs, an analysis methodology has to be designed. Since the pipes have different geometries, the Reynolds number and pressure drop are different for each case. Based on heat exchanger design [49], a criterion is needed to compare these three designs. For this purpose, a global heat transfer coefficient is defined for the systems as follows:

$$\dot{Q} = U A \Delta T_{lm}, \tag{5}$$

$$\Delta T_{lm} = \frac{(T_{PR} - T_{in}) - (T_{PR} - T_{out})}{ln\frac{(T_{PR}-T_{in})}{(T_{PR}-T_{out})}}. \tag{6}$$

The global heat transfer coefficient U provides information about the overall efficiency of the heat exchange between the system and the water flow: the higher coefficient, the more efficient the heat exchange. Hence, the cooling process.

U value alone is sufficient for comparison of heat transfer effectiveness, but this is not enough to give information about the pressure drop. The second option would be to change the mass flow rate of the cases until having the same pressure drop, but this will also affect the quantity of heat absorbed by the fluid. Therefore, by combining the idea of both criteria by using the ratio of heat absorbed and the power needed to pump the water, the following equality is considered:

$$\frac{\dot{Q}_f}{\dot{m}\Delta p} = \frac{c_p \Delta T}{\Delta p}. \tag{7}$$

This ratio tends to 0 when the mass flow rate increases because Δp will grow and ΔT will decrease for all cases. Thus, when this ratio goes to 0, a comparison of the overall heat transfer coefficient with pressure drop in consideration for all cases studied will be possible.

Fig. 14 shows the results of the global heat transfer coefficient U as a function of the ratio between the absorber heat by the fluid and the power needed to pump the water. The plot includes (logarithmic) trendlines, having a regression coefficient of about 0.99.

The design with better performance is the quarter cut with a custom heat sink in the first position, followed by the rectangular pipe with an off-the-shelf heat sink. It is also observed that when the fins are added, the increment in heat transfer is greater than the increment of pressure drop for the same comparative cases.

Fig. 14 results also indicate that within the range between double and half of the heat absorber vs. energy pump ratio, the rectangular pipe with fins presents an increase of around 23% of the global heat transfer coefficient in comparison with rectangular pipe without fins; while the quarter cut pipe shows an increase between 30% and 33% of the global heat transfer coefficient in comparison with rectangular pipe without fins.

5. Conclusions

The present paper aims to study the influence of the implementation of fins in a simple tube heat sink to achieve an optimum design for a low-cost CPV-T system. The improved heat sink pipes have been designed using a 3D Finite Volume Method model, and then they have been manufactured and tested experimentally in a laboratory test. The experimental data generated in the test rig is compared with the numerical results obtained in the simulations for validating the model, showing a reasonably good agreement. The obtained results support the accuracy of the previously implemented 3D model. The tested designs show a similar temperature difference inside the CPV Mounting Plate, within the range of 7 °C–9 °C. Then, the three heat sink designs have been simulated using the model at different flow rates, using the same inlet and material conditions to compare their overall performance. In this way, a simple comparison procedure has been used in which the overall heat transfer coefficient is plotted against the non-dimensional pumping power, i.e. the ratio between the overall transferred heat and the energy required for pumping. The result of this study revealed that the quarter cut with a custom heat sink is the best performing, with an increase of the overall heat transfer coefficient of about 60% with respect to the unfinned square tube. It is followed by the rectangular pipe with off the shelf heat sink, with an increase of about 30%. Within a range of the ratio of heat absorbed by the fluid and the power needed to pump the water between 0.7–4, the global heat transfer coefficient obtained for the quarter cut with optimized heat sink is within the range of 80–120 W/K.

Declaration of competing interest

The authors declare that they have no known competing financial interests or personal relationships that could have appeared to influence the work reported in this paper.

Data availability

Data will be made available on request.

Acknowledgements

This project has received funding from SOLAR-ERA.NET Cofund 2 joint call undertaking under the European Union's Horizon 2020 research and innovation programme. This work has also been supported by Scientific and Technological Research Council of Türkiye (TÜBİTAK) under grant number 219M028. The authors acknowledge the Heat and Environment Laboratory, Mechanical Engineering Department, METU, and the help of Bulent G. Akinoglu and Elsen Aydin. D. Santos acknowledges *FI AGAUR-Generalitat de Catalunya* fellowship (2022FI_B2_00173).

References

[1] M. Chandrasekar, T. Senthilkumar, Five decades of evolution of solar photovoltaic thermal (PVT) technology – A critical insight on review articles, J. Clean. Prod. 322 (28997) (2021) 1–18, http://dx.doi.org/10.1016/j.jclepro.2021.128997.

[2] O.Z. Sharaf, M.F. Orhan, Concentrated photovoltaic thermal (CPV-T) solar collector systems: Part I – fundamentals, design considerations and current technologies, Renew. Sustain. Energy Rev. 50 (2015) 1500–1565, http://dx.doi.org/10.1016/j.rser.2015.05.036.

[3] O.Z. Sharaf, M.F. Orhan, Concentrated photovoltaic thermal (CPV-T) solar collector systems: Part II – implemented systems, performance assessment, and future directions, Renew. Sustain. Energy Rev. 50 (2015) 1566–1633, http://dx.doi.org/10.1016/j.rser.2014.07.215.

[4] X. Ju, C. Xu, X. Han, X. Du, G. Wei, Y. Yang, A review of the concentrated photovoltaic/thermal (CPV-T) hybrid solar systems based on the spectral beam splitting technology, Appl. Energy 187 (2017) 534–563, http://dx.doi.org/10.1016/j.apenergy.2016.11.087.

[5] X. Ju, C. Xu, Z. Liao, X. Du, G. Wei, Z. Wang, et al., A review of concentrated photovoltaic-thermal (CPV-T) hybrid solar systems with waste heat recovery (WHR), Sci. Bull. FacAgric. Kyushu. Univ. 62 (2017) 1388–1426, http://dx.doi.org/10.1016/j.scib.2017.10.002.

[6] R. Daneshazarian, E. Cuce, P.M. Cuce, F. Sher, Concentrating photovoltaic thermal (CPV-T) collectors and systems: theory, performance assessment and applications, Renew. Sustain. Energy Rev. 81 (2018) 473–492, http://dx.doi.org/10.1016/j.rser.2017.08.013.

[7] A. Kasaeian, S. Tabasi, J. Ghaderian, H. Yousefi, A review on parabolic trough/fresnel based photovoltaic thermal systems, Renew. Sustain. Energy Rev. 91 (2018) 193–204, http://dx.doi.org/10.1016/j.rser.2018.03.114.

[8] J. Jacob, A.K. Pandey, N. Abd Rahim, J. Selvaraj, M. Samykano, R. Saidur, V.V. Tyagi, Concentrated photovoltaic thermal (CPV-T) systems: Recent advancements in clean energy applications, thermal management and storage, J. Energy Storage 45 (103369) (2022) 1–25, http://dx.doi.org/10.1016/j.est.2021.103369.

[9] K. Papis-Fraçzek, K. Sornek, A review on heat extraction devices for CPVT systems with active liquid cooling, Energies 15 (2022) 6123, http://dx.doi.org/10.3390/en15176123.

[10] P. Sonneveld, G. Swinkels, B.van. Tuijl, H. Janssen, J. Campen, G. Bot, Performance of a concentrated photovoltaic energy system with static linear fresnel lenses, Sol. Energy 85 (2011) 432–442, http://dx.doi.org/10.1016/j.solener.2010.12.001.

[11] T. Kerzmann, L. Schaefer, System simulation of a linear concentrating photovoltaic system with an active cooling system, Renew. Energy 41 (2012) 254–261, http://dx.doi.org/10.1016/j.renene.2011.11.004.

[12] M. Chaabane, W. Charfi, H. Mhiri, P. Bournot, Performance evaluation of concentrating solar photovoltaic and photovoltaic/thermal systems, Sol. Energy 98 (2013) 315–321, http://dx.doi.org/10.1016/j.solener.2013.09.029.

[13] R. Künnemeyer, T.N. Anderson, M. Duke, J.K. Carson, Performance of a V-trough photovoltaic/thermal concentrator, Sol. Energy 101 (2014) 19–27, http://dx.doi.org/10.1016/j.solener.2013.11.024.

[14] G. Li, G. Pei, J. Ji, M. Yang, Y. Su, N. Xu, Numerical and experimental study on a PV/T system with static miniature solar concentrator, Sol. Energy 120 (2015) 565–574, http://dx.doi.org/10.1016/j.solener.2015.07.046.

[15] H. Xie, J. Wei, Z. Wang, G. Yang, Q. Ma, Design and performance research on eliminating multiple reflections of solar radiation within compound parabolic concentrator (CPC) in hybrid CPV/T system, Sol. Energy 129 (2016) 126–146, http://dx.doi.org/10.1016/j.solener.2016.01.037.

[16] W.Ben. Youssef, T. Maatallah, C. Menezo, S.Ben. Nasrallah, Modeling and optimization of a solar system based on concentrating photovoltaic/thermal collector, Sol. Energy 170 (2018) 301–313, http://dx.doi.org/10.1016/j.solener.2018.05.057.

[17] T. Maatallah, W.Ben. Youssef, Simulation and performance analysis of concentrating photovoltaic/thermal collector (CPV/T) with three-sided thermal insulation based on coupled optothermal model, Sol. Energy 181 (2019) 308–324, http://dx.doi.org/10.1016/j.solener.2019.02.002.

[18] M. Li, X. Ji, G.L. Li, Z.M. Yang, S.X. Wei, L.L. Wang, Performance investigation and optimization of the trough concentrating photovoltaic/thermal system, Sol. Energy 85 (2011) 1028–1034, http://dx.doi.org/10.1016/j.solener.2011.02.020.

[19] E. Bellos, C. Tzivanidis, Investigation of a nanofluid-based concentrating thermal photovoltaic with a parabolic reflector, Energy Convers. Manag. 180 (2019) 171–182, http://dx.doi.org/10.1016/j.enconman.2018.11.008.

[20] A. Ustaoglu, U. Ozbey, H. Torlaklı, Numerical investigation of concentrating photovoltaic/thermal (CPV/T) system using compound hyperbolic—Trumpet, V-trough and compound parabolic concentrators, Renew. Energy 152 (2020) 1192–1208, http://dx.doi.org/10.1016/j.renene.2020.01.094.

[21] C. Renno, Experimental and theoretical analysis of a linear focus CPV/T system for cogeneration purposes, Energies 11 (2018) 2960, http://dx.doi.org/10.3390/en11112960.

[22] C. Renno, Theoretical and experimental evaluation of the working fluid temperature levels in a CPV/T system, Energies (2020) http://dx.doi.org/10.3390/en13123077.

[23] C. Renno, A. Perone, D. D'agostino, F. Minichiello, Experimental and economic analysis of a concentrating photovoltaic system applied to users of increasing size, Energies 14 (2021) 4968, http://dx.doi.org/10.3390/en14164968.

[24] D. Cabral, J. Gomes, A. Hayati, B. Karlsson, Experimental investigation of a CPVT collector coupled with a wedge PVT receiver, Sol. Energy 215 (2021) 335–345, http://dx.doi.org/10.1016/j.solener.2020.12.038.

[25] H.A. Gorouh, M. Salmanzadeh, P. Nasseriyan, A. Hayati, D. Cabral, J. Gomes, B. Karlsson, Thermal modelling and experimental evaluation of a novel concentrating photovoltaic thermal collector (CPVT) with parabolic concentrator, Renew. Energy 181 (2022) 535–553, http://dx.doi.org/10.1016/j.renene.2021.09.042.

[26] L.R. Bernardo, B. Perers, H. Håkansson, B. Karlsson, Performance evaluation of low concentrating photovoltaic/thermal systems: A case study from Sweden, Sol. Energy 85 (2011) 1499–1510, http://dx.doi.org/10.1016/j.solener.2011.04.006.

[27] F. Calise, L. Vanoli, Parabolic trough photovoltaic/thermal collectors: Design and simulation model, Energies 5 (2012) 4186–4208, http://dx.doi.org/10.3390/en5104186.

[28] M. Mohsenzadeh, M.B. Shafii, H.Jafari. Mosleh, A novel concentrating photovoltaic/thermal solar system combined with thermoelectric module in an integrated design, Renew. Energy 113 (2017) 822–834, http://dx.doi.org/10.1016/j.renene.2017.06.047.

[29] A. Moaleman, A. Kasaeian, M. Aramesh, O. Mahian, L. Sahota, G.Nath. Tiwari, Simulation of the performance of a solar concentrating photovoltaic-thermal collector, applied in a combined cooling heating and power generation system, Energy Convers. Manag. 160 (2018) 191–208, http://dx.doi.org/10.1016/j.enconman.2017.12.057.

[30] M. Shadmehri, H. Narei, R. Ghasempour, M.B. Shafii, Numerical simulation of a concentrating photovoltaic-thermal solar system combined with thermoelectric modules by coupling finite volume and Monte Carlo ray-tracing methods, Energy Convers. Manag. 172 (2018) 343–356, http://dx.doi.org/10.1016/j.enconman.2018.07.034.

[31] A. Riahi, A.B.H. Ali, A. Fadhel, A. Guizani, M. Balghouthi, Performance investigation of a concentrating photovoltaic thermal hybrid solar system combined with thermoelectric generators, Energy Convers. Manag. 205 (2019) 112377, http://dx.doi.org/10.1016/j.enconman.2019.112377.

[32] J.S. Coventry, Performance of a concentrating photovoltaic/thermal solar collector, Sol. Energy 78 (2005) 211–222, http://dx.doi.org/10.1016/j.solener.2004.03.014.

[33] N. Xu, J. Ji, W. Sun, W. Huang, Z. Jin, Electrical and thermal performance analysis for a highly concentrating photovoltaic/thermal system, Int. J. Photoenergy 2015 (2015) 537538, http://dx.doi.org/10.1155/2015/537538.

[34] N. Xu, J. Ji, W. Sun, L. Han, H. Chen, Z. Jin, Outdoor performance analysis of a 1090 × point-focus fresnel high concentrator photovoltaic/thermal system with triple-junction solar cells, Energy Convers. Manag. 100 (2015) 191–200, http://dx.doi.org/10.1016/j.enconman.2015.04.082.

[35] S. Xu, Y. Wu, O. Cai, L. Yang, Y. Li, Optimization of the thermal performance if multi-layer silicon microchannel heat sinks, Therm. Sci. 20 (6) (2016) 2001–2013, http://dx.doi.org/10.2298/TSCI141213122X.

[36] C.B. Dokken, B.M. Fronk, Optimization of 3D printed liquid cooled heat sink designs using a microgenetic algorithm with bit array representation, Appl. Therm. Eng. 143 (2018) 316–325, http://dx.doi.org/10.1016/j.applthermaleng.2018.07.113.

[37] I.K. Karathanassis, E. Papanicolaou, V. Belessiotis, G.B. Bergeles, Multi-objective design optimization of a micro heat sink for concentrating photovoltaic/thermal (CPVT) systems using a genetic algorithm, Appl. Therm. Eng. 59 (2013) 733e744, http://dx.doi.org/10.1016/j.applthermaleng.2012.06.034.

[38] I.K. Karathanassis, E. Papanicolaou, V. Belessiotis, G.B. Bergeles, Experimental and numerical evaluation of an elongated plate-fin heat sink with three sections of stepwise varying channel width, Int. J. Heat Mass Transfer 84 (2015) 16–34, http://dx.doi.org/10.1016/j.ijheatmasstransfer.2014.12.013.

[39] I.K. Karathanassis, E. Papanicolaou, V. Belessiotis, G.B. Bergeles, Design and experimental evaluation of a parabolic-trough concentrating photovoltaic/thermal (CPVT) system with high-efficiency cooling, Renew. Energy 101 (2017) 467–483, http://dx.doi.org/10.1016/j.renene.2016.09.013.

[40] R.V. Rao, K.C. More, J. Taler, P. Ocłon, Dimensional optimization of a micro-channel heat sink using jaya algorithm, Appl. Therm. Eng. 103 (2016) 572–582, http://dx.doi.org/10.1016/j.applthermaleng.2016.04.135.
[41] S. Rahmanian, H. Rahmanian-Koushkaki, P. Omidvar, A. Shahsavar, Nanofluid-PCM heat sink for building integrated concentrated photovoltaic with thermal energy storage and recovery capability, Sustain. Energy Technol. Assess. 46 (2021) 101223, http://dx.doi.org/10.1016/j.seta.2021.101223.
[42] J. Castro, J. Rigola, D. Kizildag, C. Oliet, Preliminary assessment of a poly-generation system based on a concentrated photovoltaic thermal (CPVT) solar collectors, ISHPC 2021, in: Proceedings. Part II, Technische Universität Berlin Campus Charlottenburg, http://dx.doi.org/10.14279/depositonce-12278.
[43] H.K. Versteeg, W. Malalasekera, An introduction to computational fluid dynamics, in: The Finite Volume Method, Ed., Prentice Hall, 1995.
[44] R. Felsberger, A. Buchroithner, B. Gerl, H. Wegleiter, Conversion and testing of a solar thermal parabolic trough collector for CPV-t application, Energies 13 (6142) (2020) 1–24, http://dx.doi.org/10.3390/en13226142.
[45] R. Felsberger, A. Buchroithner, B. Gerl, B. Schweighofer, H. Wegleiter, Design and testing of concentrated photovoltaic arrays for retrofitting of solar thermal parabolic trough collectors, Appl. Energy (ISSN: 0306-2619) 300 (2021) 117427, http://dx.doi.org/10.1016/j.apenergy.2021.117427.
[46] A. Buchroithner, B. Gerl, R. Felsberger, H. Wegleiter, Design and operation of a versatile, low-cost, high-flux solar simulator for automated CPV cell and module testing, Sol. Energy (ISSN: 0038-092X) 228 (2021) 387–404, http://dx.doi.org/10.1016/j.solener.2021.08.068.
[47] Official OpenFOAM website, https://www.openfoam.com/.
[48] Fujielectric study about heat sinks, 2023, https://www.fujielectric.com/products/semiconductor/model/igbt/application/box/doc/pdf/REH985b/REH985b_05.pdf [last acces: February 13th 2023].
[49] K. Ramesh, R.K. Shah, D.P. Sekulić, Fundamentals of Heat Exchanger Design, Ed., John Wiley & Sons, Inc., 2003.